THE *SWIFT* GAMMA-RAY BURST X-RAY TELESCOPE

J.E. Hill[a,b], D.N. Burrows[c], J.A. Nousek[c], A. Wells[c,d], G. Chincarini[e], A.F. Abbey[d], L. Angelini[b], A. Beardmore[d], J. Bosworth[i], H.W. Bräuninger[f], W. Chang[g], O. Citterio[e], S. Campana[e], M. Capalbi[h], P. Giommi[h], J.A. Kennea[c], R. Killough[j], B.P. Kittle[i], M. McMeekin[i], B. Miles[c], A. Moretti[e], D. Morris[c], J. Osborne[d], C. Pagani[c], A.D.T. Short[d], F. Tamburelli[h], D.J. Watson[d], R. Willingale[d], G. Tagliaferri[e], M. Zugger[c]

[a]Universities Space Research Association, 10211 Wincopin Circle, Suite 500, Columbia, MD, 21044, USA
[b]NASA/Goddard Space Flight Center, Greenbelt, MD 20771, USA
[c]Penn State University, 525 Davey Lab, University Park, PA 16802, USA
[d]Space Research Centre, University of Leicester, Leicester LE1 7RH, UK
[e]Osservatorio Astronomico di Brera, Via Brera 28, 20121 Milano, Italy
[f]Max-Planck-Institut für Extraterrestrische Physik, Garching bei München, Germany
[g]Edge Space Systems, Inc., USA
[h]ESRIN/Agenzia, Spaziale Italiana, Frascati, Italy
[i]Swales Aerospace, Inc., Beltsville, MD, USA
[j]Southwest Research Institute, San Antonio, TX, USA

The *Swift* Gamma-Ray Burst Explorer is designed to make prompt multi-wavelength observations of Gamma-Ray Bursts and GRB afterglows. The X-ray Telescope enables *Swift* to determine GRB positions with a few arcseconds accuracy within 100 seconds of the burst onset. The XRT utilizes a mirror set built for JET-X and an XMM-Newton/EPIC MOS CCD detector to provide a sensitive broad-band (0.2-10 keV) X-ray imager with an effective area of more than 120 cm^2 at 1.5 keV, a field of view of 23.6 x 23.6 arcminutes, and an angular resolution of 18 arcseconds (HPD). The detection sensitivity is $2x10^{-14}$ erg cm^{-2} s^{-1} in 10^4 seconds. The instrument provides automated source detection and position reporting within 5 seconds of target acquisition. It can also measure the redshifts of GRBs with Iron line emission or other spectral features. The XRT operates in an auto-exposure mode, adjusting the CCD readout mode automatically to optimize the science return as the source intensity fades. The XRT measures spectra and lightcurves of the GRB afterglow beginning about a minute after the burst and follows each burst for days or weeks.

We provide an overview of the X-ray Telescope scientific background from which the systems engineering requirements were derived, with specific emphasis on the design and qualification aspects from conception through to launch. We describe the impact on cleanliness and vacuum requirements for the instrument low energy response and to maintain the high sensitivity to the fading signal of the Gamma-ray Bursts.

1 INTRODUCTION

Gamma-ray bursts are brief, extremely bright flashes detected out to cosmological distances[1]. The initial blast is followed by an afterglow, which can continue for as long as months, providing important clues as to the nature of these explosive events. The *Swift* Gamma-ray Burst Explorer[2], launched in November 2004, provides a qualitative leap forward in our ability to study bursts. *Swift* detects bursts with its wide field of view gamma-ray Burst Alert Telescope[3] (BAT) and then provides unprecedented follow-up of each burst and its afterglow by slewing rapidly and autonomously to point two narrow field instruments, an X-ray Telescope[4] (XRT) and a UV-Optical Telescope[5] (UVOT), at the burst location. The X-ray Telescope rapidly refines the BAT GRB position from ~4-7 arcmin to ~5 arcsec within 5 seconds of the spacecraft settling on the burst and the UVOT, sensitive down to 24th Magnitude, can improve the burst localization to 0.3 arcsecond for those with optical afterglows. The three instruments combine to make a powerful multi-wavelength observatory (Figure 1.1, left), with the capability of rapidly determining the positions of GRBs to arcsecond accuracy within 1-2 minutes of their discovery, and the capability of measuring both lightcurves and redshifts of the bursts and afterglows. The GRB positions, lightcurves and quick-look spectra obtained by the three instruments are telemetered autonomously and immediately from the *Swift* spacecraft to Tracking and Data Relay Satellites (TDRSS) for rapid transmission to the GRB Co-ordinate Network (GCN). Email messages containing those data are automatically delivered throughout the world to GRB scientists and to telescopes for GRB follow-up.

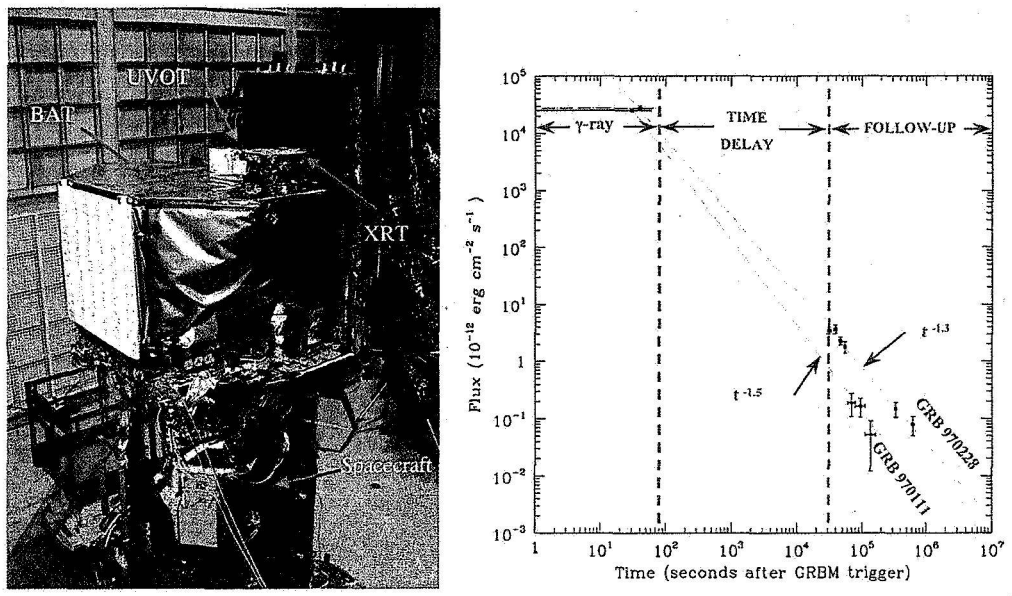

FIGURE 1.1. ***Left: The Swift Observatory in a class 10 000 cleanroom during the integration and test phase at the NASA/Goddard Space Flight Center. The three instruments are mounted on the optical bench with several of the electronics boxes and the sun-shield. The solar arrays are not yet installed. Right: Two typical GRB lightcurves in the pre-swift era, where there were limited observations of the GRB afterglow until around 10 000 seconds after the initial prompt gamma-ray emission.***

2 OVERALL DESCRIPTION

It is generally accepted that the GRB early emission detected by gamma-ray telescopes, is synchrotron emission from a power law distribution of electrons in a highly relativistic outflow[1]. The short-term variability of flux with time is thought to be due to the collision of faster and slower moving shells, causing internal shock-waves. The afterglow, detected at later times, is attributed to the deceleration of the relativistic fireball colliding with the interstellar medium. Typically, by the time that previous missions were able to observe a typical X-ray afterglow (~10 000 seconds), the afterglow intensity had already dropped by 4-5 orders of magnitude (Figure 1.1., left). The concept for *Swift* was to fill in the large time gap (100-10 000 seconds) using the XRT and to provide accurate positions within 5 seconds of target acquisition for typical bursts, allowing ground-based optical telescopes to begin immediate spectroscopic observations of the afterglow. The *Swift* XRT is a sensitive, flexible, autonomous X-ray imaging spectrometer designed to measure fluxes, spectra, and lightcurves of gamma-ray bursts (GRBs) and afterglows over a wide dynamic range covering more than 7 orders of magnitude in flux.

2.1 Science Requirements

The XRT design was derived from the following science requirements:

- **GRB X-ray Position Accuracy**
  Rapid, accurate positions are required for ground-based follow-up. The XRT is required to report GRB positions with better than 5" accuracy to the ground within 100 seconds of the GRB detection. 95 seconds are allocated to the BAT position calculation and to the spacecraft for slewing; allowing 5 seconds for XRT to autonomously determine the GRB position[6].
- **X-ray Spectroscopy**
  Good spectral resolution is required for redshift measurements. The XRT was designed with an expected end-of-life (3 yrs after launch) energy resolution of less than 400 eV full-width at half maximum at 6 keV. This required a beginning of life resolution of better than 150 eV.
- **Sensitivity**
  Long-term follow up is required to look for spectral changes and time variability to determine the origin and the local environment of GRBs. The XRT was designed to detect sources as weak as 2×10^{-14} ergs/cm^2/s in 10 000 seconds in the 0.2-10 keV energy band.
- **Measure Light-curves**
  Short time-scale variability provides important clues to GRB and afterglow physical processes and environments. By autonomously switching between different readout modes the XRT provides high-time resolution of at least 10 ms when the source is bright, and high sensitivity when the source is faint[6].

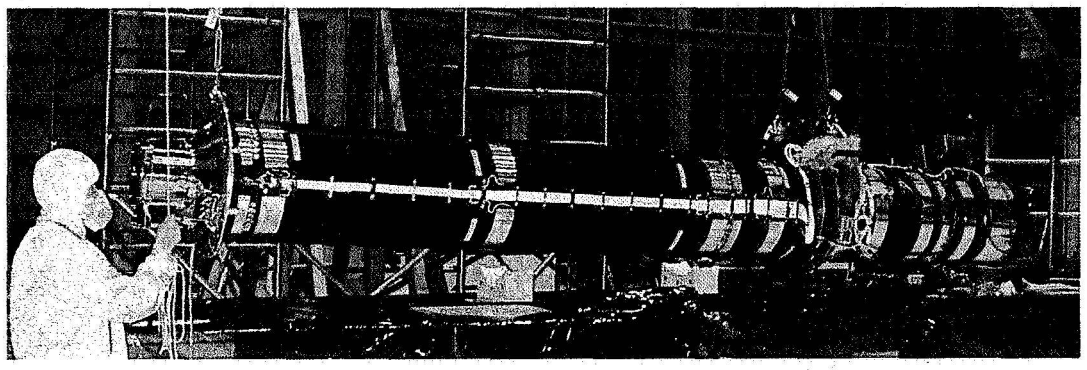

FIGURE 2.1. ***The XRT inside the SSDIF cleanroom at the NASA GSFC during instrument integration and test. The two silver rings are ground support equipment for performing a horizontal lift of the instrument. The gold colored ring in the center is the OBIF.***

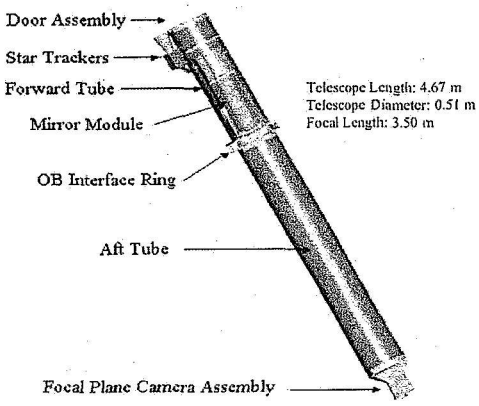

Telescope	3.5m Wolter I
Telescope PSF	15 arcsec HPD @ 1.5 keV 20 arcsec HPD @ 8.1 keV
Detector	MAT CCD-22
Detector Format	600 x 600 pixels
Detector Readout Modes	Photon-counting, Imaging, & Timing
Field of View	23.6 x 23.6 arcmin
Pixel Scale	2.36 arcsec / pixel
Energy Range	0.2 - 10 keV
Effective Area	110 cm^2 @ 1.5 keV
Sensitivity	2 x 10^{-14} ergs/cm^2/s in 10^4 s
Position Accuracy	2.5 arcseconds
Operation	Autonomous

FIGURE 2.2. ***Left: Diagram of the XRT telescope sub-system showing the relative positions of the main components. Right: A table of the XRT instrument parameters.***

3 INSTRUMENT DESCRIPTION

3.1 Structure

The layout of the XRT is shown in Figure 2.1 and Figure 2.2, and the instrument is shown mounted on the *Swift* Instrument Module in Figure 1.1. The XRT structure is designed around the Optical Bench Interface Flange (OBIF), with the forward telescope tube supporting the star trackers and the XRT door module and the aft telescope tube supporting the Focal Plane Camera Assembly (FPCA).

Optical Bench Interface Flange: The OBIF is the primary structural element of the XRT and is responsible for supporting the forward and aft telescope tubes, the mirror module, and the electron diverter. It also provides the interface to the *Swift* Optical Bench.

Telescope Tube: The 508 mm diameter carbon fiber tube, manufactured by ATK, is composed of two sections. The carbon fiber lay-up is designed to give the tube a negligible longitudinal CTE so that temperature gradients will not adversely effect the alignment or focus, required for accurate positions. The composite tube is lined with an aluminum foil vapor barrier to guard against outgassing of water vapor or epoxy contaminants into the telescope interior. The rear section incorporates a flange at its forward end, which mates to the OBIF and a flange at its rear end, which mates to the FPCA, and incorporates internal optical baffles. The forward telescope tube section encloses the mirrors and supports the door module and the star trackers.

Door: The telescope tube is sealed at the forward end by a door designed to protect the X-ray mirrors from contamination during ground operations and launch.

3.2 Optics

The XRT mirror assembly consists of the X-ray mirror module (Figure 3.1.. left), a thermal baffle mounted in front of the mirrors, a mirror collar that mates to the OBIF, and an electron diverter that mounts behind the mirrors (Figure 3.1., right).

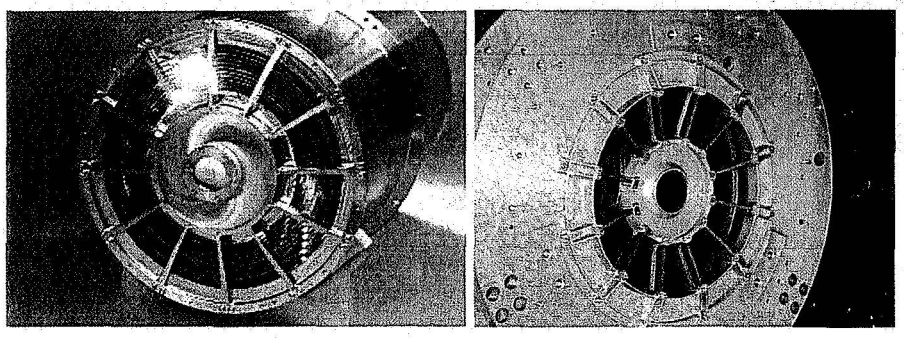

FIGURE 3.1. Left: XRT mirror module, depicting the 12 mirror shells inside the mirror casing. Right: The XRT electron diverter mounted inside the OBIF.

XRT Mirrors: The XRT uses the FM3 mirror set built and calibrated for the *JET-X* program[7,8] (Figure 3.1., left). The effective area and point spread function of the mirrors have been measured for a variety of energies and off-axis angles, and were recalibrated with the instrument at the Max Planck Institute für Extraterrestrische Physik Panter Facility in July 2000[9].

Thermal Baffle: A thermal baffle in front of the mirror prevents temperature gradients in the mirror that can distort the mirror and degrade the Point Spread Function (PSF), reducing the position accuracy. The baffle temperature is actively controlled by heaters, which balance the heat lost to space by the mirrors.

Electron Diverter: The electron flux in the 600 km, 22° inclination orbit will produce a time-varying detector background. An electron diverter (Figure 3.1. Right), consisting of a system of rare earth magnets, is installed on the OBIF near the rear face of the mirrors to prevent electrons from reaching the detector. These magnets are arranged to have a near-zero dipole moment.

3.3 Focal Plane Camera Assembly

The XRT Focal Plane Camera Assembly (Figure 3.2., left) shields the CCD against trapped protons and cosmic rays, and provides cooling for the detector via a coldfinger to the heatpipes. The cryostat provided a vacuum environment in which the CCD could be cooled for ground testing without the build-up of moisture, and also limited the build-up of contamination during integration and test and during launch and early orbit operations. The cryostat has a single-shot door opening mechanism, utilizing redundant *Starsys* High Output Paraffin (HOP) mechanisms.
The cryostat is attached to a conical interface section (Figure 3.2., left), which mounts onto the rear tube, supports the cryostat, door control hardware and radiator interface, and incorporates a baffled venting system. The vent port allows the telescope internal volume to vent during launch and vacuum testing, while preventing scattered light from entering the CCD enclosure.

Optical Blocking Filter: A thin filter is installed in front of the CCD to block optical light consisting of a single fixed polyimide film 1840 Å thick, coated on one side with 488 Å of aluminum. The optical transmission of the filter is about 2.5×10^{-3}. The filter, positioned in front of the field of view of the CCD, limits background light from getting to the detector, contaminating the X-ray signal and reducing the sensitivity. It is extremely fragile. For the venting of the FPCA to atmosphere and the opening of the FPCA door extra caution was taken to limit the pressure differential so that the filter was not damaged in any way, as optical light and background variations due to light leaks severely limit the energy resolution of the detector. If the filter were damaged, short circuits from metallic particles on the detector could cause complete failure of the instrument.
The filter is also susceptible to damage from solar illumination. To prevent damage to the filter (melting) in the event of loss of attitude control and illumination of the filter by the sun, there is a sun-shutter activated by a Ga-As array of solar cells mounted at the top of the mirror baffle, which provide power to the sun-shutter electronics if the spacecraft slews to within 30 degrees of the Sun, even if the instrument is turned off. If the XRT is pointed closer than 10 degrees to the Sun, the sun-shutter is automatically actuated. It can also be opened or closed manually.

CCD Architecture: The CCD-22 detector, designed for the *EPIC* MOS cameras on *XMM-Newton* by the company formerly known as EEV, is a three-phase frame-transfer device, which utilizes high resistivity silicon and an open-electrode structure[10] to achieve a useful bandpass of 0.2 to 10 keV[11]. It has an imaging area of ~2.4 x 2.4 cm. The image section of each CCD is a 600 x 602 array of 40μm x 40μm pixels, each pixel corresponding to 2.36 arcseconds in the *Swift* focal plane. The storage region is a 600 x 602 pixel array, of 39 x 12 μm pitch. The readout register is split

into two sections, and is read out using either output node. The CCD is operated in four different modes: Photodiode mode or windowed timing mode, which allow a faster readout of fewer pixels so that bright sources may be observed without saturation and to achieve high-timing resolution; image mode to obtain the GRB position or photon-counting mode for maximum sensitivity[6,12].

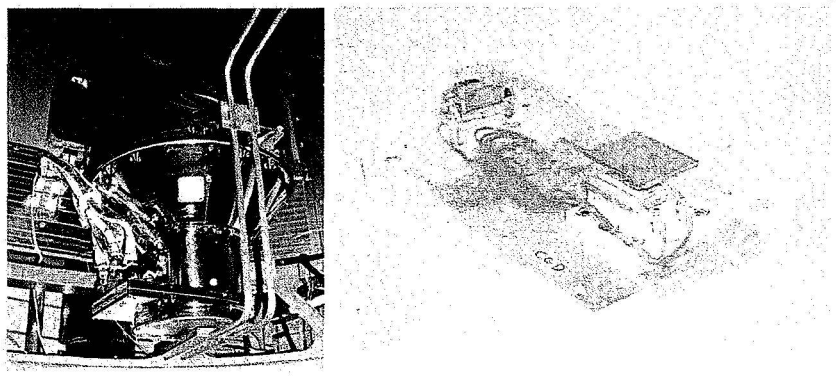

FIGURE 3.2. ***Left: The FPCA attached to the aft telescope tube inside the Swift spacecraft. Two heat-pipes conduct the heat from the hot-side of the TEC out to a radiator externally mounted to the spacecraft. Right: The CCD-22 mounted on top of the TEC prior to integration into the FPCA.***

4 INTEGRATION AND TEST

Prior to launch the XRT subsystems, instrument and the *Swift* observatory were subjected to the tests outlined in Table 4.1. Several of the XRT subsystems are particularly sensitive to contamination and therefore the environment of the instrument and spacecraft were controlled throughout the manufacture, integration and environmental tests and also during the early on-orbit operations to minimize particulate and molecular contamination levels.

TABLE 4.1. ***Tests performed at the various stages of integration and critical on-orbit tests.***

Sub-system Tests	Instrument Tests	Spacecraft Tests	On-Orbit Critical Activites
Vibration	Vibration	Vibration	Outgassing
Bake-out	Thermal Cycles	Thermal Cycles	Slew tests
Thermal Cycles	Thermal Balance	Thermal Balance	Fwd Tube door opening
Functional	Calibration	EMI/EMC	Camera door opening
	EMI/EMC	Day-in-the-life	Detector cooling

Molecular Contamination: The performance of the XRT mirrors, optical blocking filter, and CCD can be degraded by the deposition of outgassed products. The low-energy X-ray spectral response is particularly sensitive to very small changes in optical properties caused by the deposition of outgassed products. Major sources of molecular contamination are listed below.

a. Lubricants, leaks, and exposed organic materials may emit volatile condensable materials, which can be subsequently transferred to critical surfaces. The CCD detector and filter are generally significantly colder than the surrounding hardware and therefore are particularly susceptible. Exposure of contamination sensitive hardware to volatile condensable materials was restricted during all operations.

Particulate Contamination: Detector performance degradation can also be caused by off-axis radiation scattering due to particle clouds and enhancement of mirror scattering reflectance due to surface particulate contaminants. Major sources of particulate contamination are listed below.

a. Airborne particles settling on hardware surfaces during manufacturing, assembly, and test activities.
b. Paint overspray, insulation shreds, clothing fibers, and other human induced substances.
c. Trapped particles on the internal surfaces of subassemblies and other hardware crevices that are released and re-dispersed from acoustic vibration, transportation, launch, and on-orbit activities.
d. Personnel working on or near hardware are also sources of contamination to critical surfaces. These sources include skin, hair, vapors, and fingerprints.
e. Particles from the launch vehicle fairing materials and/or trapped by the fairing blankets can be re-dispersed during launch and can degrade the exterior surfaces of the *Swift* Observatory.
f. Particles from the launch vehicle pyrotechnic devices are also sources of particulate contamination and can degrade the exterior surfaces of the *Swift* Observatory.

To avoid the build up of contaminants on surfaces, which could easily migrate to critical hardware, component hardware was subjected to cleaning and/or bakeout to stringent levels, prior to every level of integration.

To limit the effect of any residual contamination, prior to cooling the detector during the thermal vacuum tests, the spacecraft was allowed to outgas for 24 hours until the chamber pressure reached an acceptable level and the protective cryo-plates had reached temperature. The forward tube door remained closed during the spacecraft tests, and the camera door was only opened at the end of the final thermal cycle, ~ 3 weeks. A similar process was followed on orbit. The forward tube door was opened 18 days after launch, giving the spacecraft time to outgas before exposing the mirrors. The tube was then allowed to outgas for four more days before opening the camera door. The CCD detector was heated via the Thermo-Electric Cooler (TEC) to a temperature above that of the surrounding area when the camera door was opened, so that any remaining contaminants would not be attracted to the detector surface. Unfortunately, just prior to the planned cooling of the CCD to its operation temperature, the CCD closed-loop thermal control system failed.
Throughout testing and transportation, the telescope tube and the interior of the spacecraft waere continuously purged to a positive pressure with ultra clean dry Nitrogen.
The vent port, which allowed the release of pressure inside the telescope tube, remained plugged until just prior to TVAC operations and launch.

Moisture Build-up: The performance of the CCD X-ray detector is sensitive to build-up of water or ice on the CCD surface. The presence of water (ice or liquid) reduces the soft X-ray response and over time will invalidate calibrations. The XRT was designed with the facility to heat the CCD to drive off any residual water. During integration and test the FPCA remained under vacuum where possible, using a non-oil based diaphragm pump and a turbo pump. This served several purposes. It maintained a cleaner environment and limited the build up of contaminants on to the critical interior surfaces, allowed the cooling of the detector with the TEC during performance and verification tests, and provided a pre-launch (and pre-TVAC) vacuum for the interior of the camera limiting the acoustic load on the fragile optical blocking filter.

5 ON-ORBIT PERFORMANCE AND ISSUES

The *Swift* observatory slewed to a GRB autonomously for the first time on 17th January 2005[13]. Figure 5.2 shows the BAT lightcurve, uncorrected for background, and the XRT image obtained 193 seconds after the burst triggered the BAT. The burst was so bright at the time of acquisition that the XRT only required an integration of 0.1 seconds to determine the GRB position autonomously onboard. Following the determination of the GRB position the XRT autonomously switches between four readout modes depending on the source flux in order to optimize the science return. Figure 5.2 shows a lightcurve obtained from two of the XRT modes and also of the BAT lightcurve extrapolated into the XRT bandpass for GRB 050904[14].

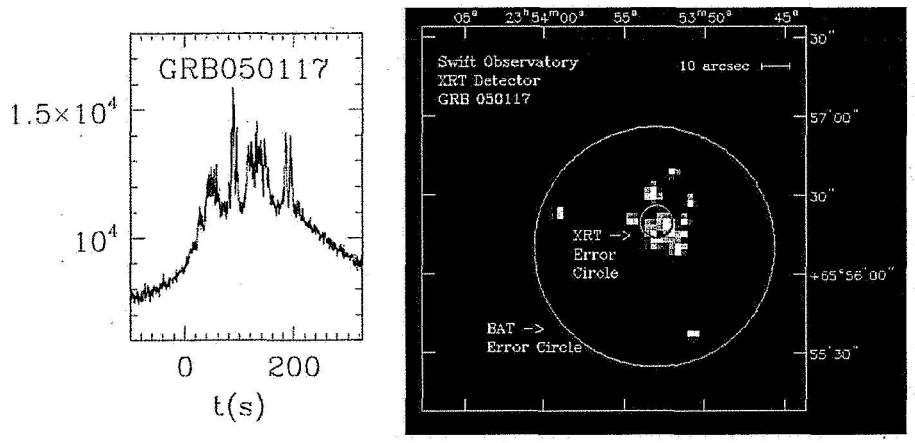

FIGURE 5.1. GRB 050117, was the first burst to which Swift autonomously slewed and for which the XRT determined a GRB position within 5 seconds of the spacecraft settling on the burst. Left: The BAT lightcurve uncorrected for background. Right: The X-ray image of the GRB integrated for 0.1 seconds, and the corresponding error circles for the BAT position and the XRT position.

Optimizing the operation of the XRT on-orbit has been a continuous effort. The loss of the controlled cooling system, which was designed to maintain the CCD temperature at -100 +/- 1 °C, has lead to relying only on the passive cooling from the radiator and duel-heat-pipes. This maintains the overall CCD temperature between -75 and -50 °C with a +/- 4 °C orbital variation[15]. Due to the versatile flight software, the data obtained from burst chasing are still meeting (and exceeding) the science requirements.

At 5:22 UT on 28th May 2005, an event occurred on-orbit causing anomalously high countrates in the CCD. This event, believed to be micro-meteroid impact, has left permanent damage to the CCD in the form of several hot

columns (Figure 5.3). The brightness of these columns is temperature dependent and at higher temperatures the charge occasionally floods into the adjacent columns. The effect of the damage has been mitigated within the flight software, with only the loss of these columns.

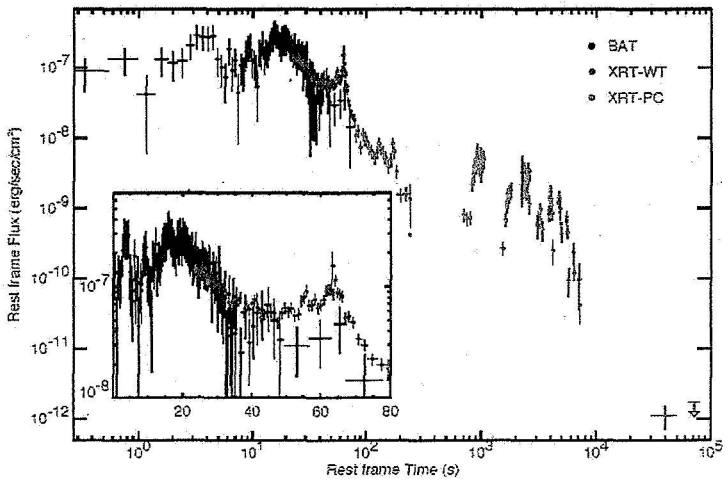

FIGURE 5.2. A joint BAT and XRT lightcurve for GRB 050904, the furthest GRB detected to date at a redshift of 6.29. The BAT data is extrapolated into the XRT bandpass; 0.2-10 keV. This lightcurve shows flaring activity out beyond 1000 seconds, which is very unusual.

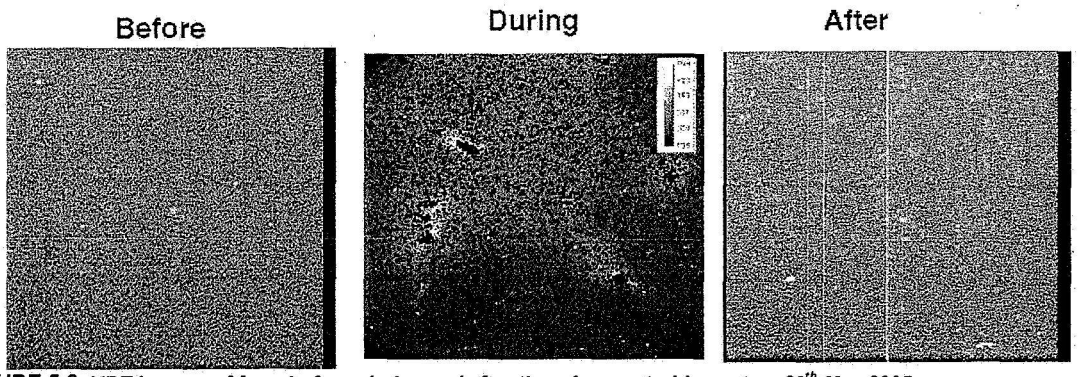

FIGURE 5.3. XRT images of from before, during and after the micro-metroid event on 28th May 2005.

6 CONCLUSION

The *Swift* Gamma-ray burst explorer has exceeded all of its pre-launch science goals, localizing several short GRBs and detecting the most distant *and* one of the closest cosmic explosions ever observed. From filling in the 'data gap' between ~100 and 10 000 seconds, the XRT has discovered unexpected early time afterglow behaviors. Although *Swift* has detected more than 100 bursts to date, due to each burst being different, many more observations are needed to understand these elusive events.

This work is supported at Penn State by NASA contract NAS5-00136; at the University of Leicester by funding by the Particle Physics and Astronomy Research Council on grant number PPA/Z/S/2003/00507; and at OAB by funding from ASI on grant I/R/039/04. We gratefully acknowledge the contributions of dozens of members of the *Swift* team at PSU, University of Leicester, OAB, GSFC, ASDC, Panter, SwRI and Swales who helped make this Observatory possible.

7 REFERENCES

1. B. Zhang and P. Meszaros, "Gamma-ray Bursts: Progress, Problems and Prospects", *Int. J. Mod. Phys. A.*, 19, 2385 (2004)
2. N. Gehrels, et al., "The Swift Gamma-ray Burst Mission", *ApJ.*, 611, 1005 (2004)
3. S.D. Barthelmy *et al.*, "The Burst Alert Telescope (BAT) on the Swift MIDEX mission" *Space Science Review*, 120, 143 (2005)

4. D.N. Burrows *et al.* "The Swift X-ray Telescope", *Space Science Review*, 120, 165 (2005)
5. P.W.A. Roming *et al.*, "The Swift UV-Optical Telescope", *Space Science Review*, 120, 195 (2005)
6. J.E. Hill *et al.*, "Readout modes and automated operation of the Swift X-ray Telescope", *Proc. SPIE*, 5165, 217 (2004)
7. O. Citterio *et al.*, "Characteristics of the flight model optics for the JET-X telescope onboard the SPECTRUM X-γ satellite", *Proc. SPIE,* 2805, 56 (1996)
8. A. Wells *et al.*, "X-ray Imaging Performance of the Flight Model JET-X Telescope", *Proc. SPIE*, 3114, 392 (1997)
9. A. Moretti *et al.*, "In-flight calibration of the Swift XRT Point Spread Function", *Proc. SPIE,* 5165, 360 (2005)
10. A. D. Holland *et al.*, "MOS CCDs for the EPIC on XMM", *Proc. SPIE,* 2808, 414 (1996)
11. A .D. T. Short, A. Keay and M. J. L. Turner, "Performance of the XMM EPIC MOS CCD Detectors", *Proc. SPIE,* 3445, 13 (1998)
12. J. Osborne *et al.*, "The in-flight spectroscopic performance of the Swift XRT CCD camera", *Proc. SPIE,* 5165, 352 (2005)
13. J.E. Hill *et al.*, "GRB 050117: Simultaneous Gamma-Ray and X-Ray Observations with the Swift Satellite", *ApJ.*, 639, 303 (2006)
14. G. Cusumano *et al.*, "Gamma-ray bursts: Huge explosion in the early Universe", *Nature*, Vol. 440, Issue 7081, 164 (2006)
15. J.A. Kennea *et al.*, "Controlling the Swift XRT CCD temperature via passive cooling", *Proc. SPIE*, 5898, 341 (2005)